Microfluidic-Synthesized Amorphous Calcium Phosphate Nanoparticles Enhance Osteogenesis, Suppress Osteoclastogenesis, and Promote Bone Healing in a Murine Femoral Defect Model

Bei Liu[1,2,3], Gianna Smolock[4], Hani Awad[1,2,3]
[1]Center for Musculoskeletal Research, [2]University of Rochester, [3]University of Rochester Medical Center, Rochester, NY
[4]Wesleyan University, Middletown, CT
bei_liu@urmc.rochester.edu

Disclosures: Bei Liu (N), Gianna Smolock (N), Hani Awad (N)

INTRODUCTION: Critical-sized bone defects resulting from trauma, tumor, or osteomyelitis remain a major challenge in orthopedic reconstruction, costing $2.5 billion annually.[1] Traditional autografts are limited by donor site morbidity and limited availability, while allografts and xenografts present risks of immune rejection and disease transmission.[2] Although 3D-printed calcium phosphate scaffolds are common graft substitutes, they often lack biomechanical strength and osteoinductivity. To overcome these limitations, we previously developed carboxymethyl chitosan (CMC)/amorphous calcium phosphate (ACP) nanoparticles (NPs), which can be 3D printed into PCL scaffolds to regenerate bone in critical-sized radial defects in rats.[3] We subsequently optimized and scaled up NP synthesis via a microfluidic system, enabling precise control of particle size, surface charge, and overall yield.[4] Here, we investigated the effects of microfluidic-synthesized CMC/ACP NPs, incorporated into 3D-printed polycaprolactone (PCL) scaffolds, on osteogenesis, osteoclastogenesis, and bone regeneration in a mouse femoral defect.

METHODS: CMC/ACP NPs were synthesized using a microfluidic chip, purified by dialysis, and characterized by dynamic light scattering (DLS) and scanning electron microscopy (SEM) as previously described (Fig. 1A).[4] Lyophilized NP powder was incorporated into PCL (3:1 NP: PCL) and 3D-printed into cylindrical scaffolds. Cytocompatibility and osteogenesis were evaluated in murine ST2 stromal cells using CCK-8, alkaline phosphatase (ALP), Alizarin Red S (ARS), and RT-PCR. Osteoclastogenesis was assessed in bone marrow macrophages treated with M-CSF/RANKL ± NPs using TRAP staining, F-actin, NF-κB, NFATc1, and resorption pits. To investigate the NP osteoregenerative properties in vivo, female BALB/cJ mice (n=3/group) underwent survival surgery to create 3-mm femoral defects, which were reconstructed with PCL or PCL+NP scaffolds. All animal work was approved by IACUC. Female mice were used to minimize variability, only one sex was selected to avoid hormonal effects. Bone formation was assessed quantitatively using X-ray and micro-CT at 0, 1, 2, and 3 months, respectively. Statistics: Analysis of variance with Bonferroni-corrected post-hoc multiple comparisons or unpaired t-tests were used to assess in vitro and in vivo effects, respectively, with p-values ≤ 0.05 deemed statistically significant.

RESULTS: CMC/ACP NPs averaged 120.9 nm (PDI 0.17, zeta potential –19.9 mV) and were stable over 6 months. SEM showed uniform, spherical particles. NPs were cytocompatible and did not reduce viability of ST2 or BMM cells. In ST2 cells, NP treatment enhanced mineralization in a dose-dependent manner, with the highest ARS staining at 500 μg/mL at days 14 and 21 (Fig. 1B). ALP activity peaked at day 7 and was unchanged by NP. PCR showed significant upregulation of RUNX2, OSX, COL1A, ALPL and OCN at higher NP doses and later time points (Fig. 1C). Osteoclast assays demonstrated a dose-dependent reduction in TRAP+ cells (Figure 2A, D), resorptive pits (Figure 2B, D), with near-complete inhibition at 500 μg/mL, accompanied by dose-dependent decrease in NF-κB and NFATc1 nuclear localization (Figure 2C, D). In vivo, both scaffold groups supported bone formation, but PCL-only scaffolds formed bone mainly at defect margins, leaving a central void, whereas PCL+NP scaffolds showed mineralization throughout and around the scaffold (Fig. 3A). Incremental bone formation analysis showed a trend toward higher monthly new bone volume in the NP group, especially at months 2–3 (Figure 3B,C).

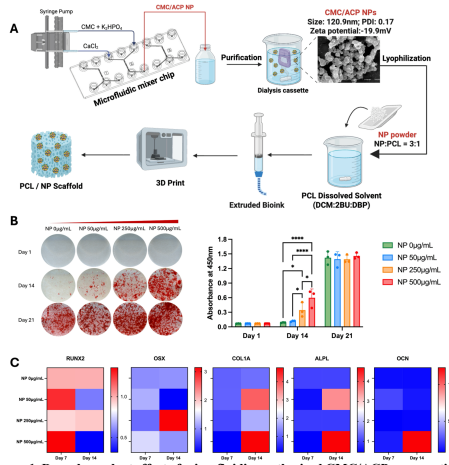

Figure 1. Dose-dependent effect of microfluidic-synthesized CMC/ACP nanoparticles on osteogenesis in ST2 stromal cells. (A) Schematic of microfluidic synthesis of CMC/ACP nanoparticles and extrusion-based fabrication of 3D-printed PCL/NP scaffolds. (B) Alizarin Red S (ARS) staining at days 14 and 21 demonstrated a dose-dependent increase in mineral deposition, with the highest calcium accumulation at 500 μg/mL. (C) Quantitative PCR analysis revealed upregulation of osteogenic genes (RUNX2, OSX, COL1A, ALPL, OCN) at higher NP concentrations and later time points. Data are presented as mean ± SD (n = 3); $p < 0.05$ indicates statistical significance between groups.

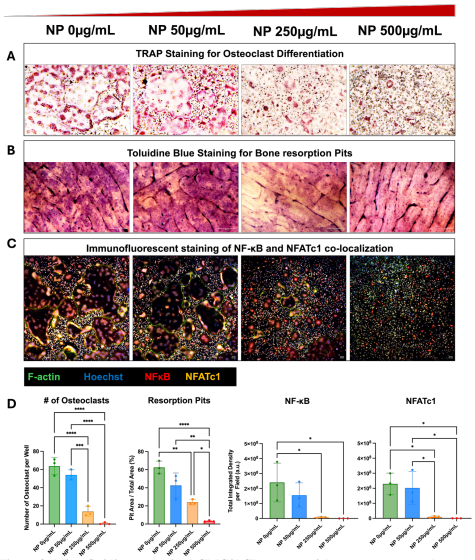

Figure 2. Microfluidic-synthesized CMC/ACP nanoparticles suppress osteoclast formation and resorptive activity in a dose-dependent manner. (A) TRAP staining of bone marrow macrophages (BMMs) cultured with M-CSF (50 ng/mL) and RANKL (50 ng/mL) ± NPs (0, 50, 250, 500 μg/mL) for 5 days. (B) Toluidine blue staining of bovine bone slices showing resorptive pits. (C) Representative immunofluorescence images showing nuclear NF-κB and NFATc1 localization. (D) Quantification of TRAP-positive osteoclast number per well, resorbed pit area per ROI, NF-κB integrated density per field, and NFATc1 integrated density per field, respectively. Data are presented as mean ± SD (n = 3); $p < 0.05$ indicates statistical significance between groups.

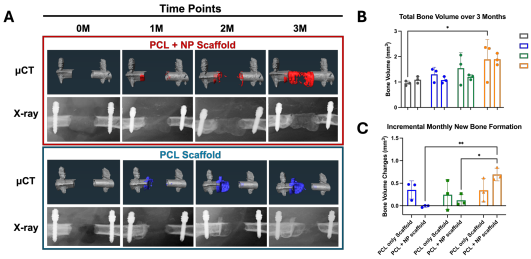

Figure 3. Microfluidic-synthesized CMC/ACP nanoparticle–loaded scaffolds promote robust mineralization in a murine femoral defect model. (A) Representative X-ray and micro-CT images at 0-, 1-, 2-, and 3-months post-surgery. (B) Quantitative analysis of total bone volume over 3 months. (C) Incremental monthly new bone formation calculated from sequential bone volume measurements. Data are presented as mean ± SD (n = 3); $p < 0.05$ indicates significance between groups.

DISCUSSION: Microfluidic-synthesized CMC/ACP nanoparticles embedded in 3D-printed PCL scaffolds enhanced osteogenesis and suppressed osteoclastogenesis, yielding improved mineralization in murine femoral defects than PCL alone. This effect is likely mediated by ACP-derived calcium and phosphate ion release that upregulates osteogenic programs in MSCs and inhibits NF-κB/NFATc1 signaling in pre-osteoclasts. It is also possible that the CMC shell contributes to these effects. This manufacturable approach yields tighter size and surface charge consistency and prolonged storage stability with potential to scale up for clinical applications by arraying microfluidic synthesis. However, the study remains preliminary, and future work will optimize NP loading in the PCL scaffolds, increase sample size, include biomechanical testing endpoints, and pursue mechanistic experiments to determine the relative contributions of calcium and phosphate ions and the CMC shell of the NPs.

CLINIAL RELEVANCE: This work offers a manufacturable strategy to accelerate bone repair and stabilize challenging segmental defects. If validated in large-animal models, this off-the-shelf, non-biologic scaffold could reduce nonunion risk in critical-sized long bone defects.

ACKNOWLEDGEMENTS: We would like to acknowledge NIH/NIAMS (P50AR072000 and P30AR069655).

REFERENCES: [1] Wang W, et al. *Bioact Mater*. 2017. [2] Oryan A, et al. *J Orthop Surg Res*. 2014. [3] Yan M, et al. *Bioact Mater*. 2025. [4] Liu, B. et al. ORS 2025 Annual Meeting Paper No. 763.